Applied Numerical Mathematics 128 (2018) 139–156

Contents lists available at ScienceDirect

Applied Numerical Mathematics

www.elsevier.com/locate/apnum

Regularized linear schemes for the molecular beam epitaxy model with slope selection

Lizhen Chen [a], Jia Zhao [b,*], Xiaofeng Yang [c,d]

[a] Beijing Computational Science Research Center, Beijing, China
[b] Department of Mathematics & Statistics, Utah State University, Logan, UT, USA
[c] Department of Mathematics, University of South Carolina, Columbia, SC 29208, USA
[d] School of Mathematical Sciences, University of Electronic Science and Technology of China, Chengdu, 610054, China

ARTICLE INFO

Article history:
Received 6 August 2017
Received in revised form 8 January 2018
Accepted 4 February 2018
Available online 8 February 2018

Keywords:
Phase field
Molecular beam epitaxy
Energy stable
Linear scheme

ABSTRACT

In this paper, we propose full discrete linear schemes for the molecular beam epitaxy (MBE) model with slope selection, which are shown to be unconditionally energy stable and unique solvable. In details, using the invariant energy quadratization (IEQ) approach, along with a regularized technique, the MBE model is first discretized in time using either Crank–Nicolson or Adam–Bashforth strategies. The semi-discrete schemes are shown to be energy stable and unique solvable. Then we further use Fourier-spectral methods to discretize the space, ending with full discrete schemes that are energy-stable and unique solvable. In particular, the full discrete schemes are linear such that only a linear algebra problem need to be solved at each time step. Through numerical tests, we have shown a proper choice of the regularization parameter provides better stability and accuracy, such that larger time step is feasible. Afterward, we present several numerical simulations to demonstrate the accuracy and efficiency of our newly proposed schemes. The linearizing and regularizing strategy used in this paper could be readily applied to solve a class of phase field models that are derived from energy variation.

1. Introduction

Molecular beam epitaxy (MBE) is an epitaxy method for thin-film deposition of single crystals. So far quite a few mathematical models as well as the accompanying numerical simulation tools have been developed to study dynamics of the MBE growth process [3,5,16,20,21,36,45]. For the continuum model, there are several approaches developed to model molecular beam epitaxy growth. One popular approach is the energy-variational based. In [12], Golubovic introduces the effective free energy formation of the MBE growth model (without slope selection); and in [30], Moldovan and Golubovic introduce the MBE growth model (with slope selection), where the anisotropic MBE models are also considered (affecting the coarsening dynamics). Notice that there are many other cases, where the surface motion could not be generated by an effective free energy functional [13,23–27].

Given the effective free energy, we present the MBE growth model and discuss its energy dissipation properties which serve as a guideline for us developing numerical schemes. Let $\phi(x,t)$ be the epitaxy surface height with $x \in \Omega$, where Ω is a

* Corresponding author.
E-mail addresses: lzchen@csrc.ac.cn (L. Chen), jia.zhao@usu.edu (J. Zhao), xfyang@math.sc.edu (X. Yang).

https://doi.org/10.1016/j.apnum.2018.02.004
0168-9274/

confined domain in R^2. Under typical conditions for MBE growth, the height (ϕ) evolution equation is given in a relaxation dynamical form of a L^2 gradient flow:

$$\phi_t = -M\frac{\delta E}{\delta \phi}, \tag{1.1}$$

where M is the mobility coefficient, E is the effective free energy (which represents the kinetic asymmetry in attachment and detachment of adatoms to and from terrace boundaries [28]) and $\frac{\delta E}{\delta \phi}$ denotes the variational derivative of E with respect to ϕ.

For the effective free energy, two widely used phenomenological expressions are as follows: (1) with slope selection expression [30]

$$E(\phi) = \int_\Omega \Big(\frac{\varepsilon^2}{2}(\Delta\phi)^2 + \frac{1}{4}(|\nabla\phi|^2 - 1)^2\Big)d\Omega, \tag{1.2}$$

and without slope selection expression [12]

$$E(\phi) = \int_\Omega \Big(\frac{\varepsilon^2}{2}(\Delta\phi)^2 - \frac{1}{2}\ln(1 + |\nabla\phi|^2)\Big)d\Omega, \tag{1.3}$$

where ε is a constant (inversely proportional to the size of the system). A detailed discussion of differences between these two free energies could be found in [28]. In short, the first term in the free energy represents the surface diffusion effect and the second term represents a continuum description of the effect that the adatoms (absorbed atoms) must overcome a higher energy barrier to stick to a step from an upper rather than from a lower terrace. After substituting the expression of free energy (1.2) and (1.3) into the model (1.1), we obtain the two nonlinear MBE models: (1) MBE model with slope selection

$$\partial_t\phi = -M\Big(\varepsilon^2\Delta^2\phi - \nabla\cdot((|\nabla\phi|^2 - 1)\nabla\phi)\Big), \tag{1.4}$$

and (2) MBE model without slope selection

$$\partial_t\phi = -M\Big(\varepsilon^2\Delta^2\phi - \nabla\cdot(\frac{\nabla\phi}{1 + |\nabla\phi|^2})\Big). \tag{1.5}$$

A feature of the continuum MBE models considered in this paper, i.e. (1.4) and (1.5), is that it is derived from an energy variational approach and thereby satisfies an energy dissipation law (or thermodynamically consistent). The energy dissipation law, in fact, serves as a guide for the design of thermodynamically consistent (energy stable) numerical schemes. In practice, it is especially desirable in the design of numerical schemes that preserve the energy dissipation property at the discrete level. On the one hand, the preservation of the energy law is critical for the numerical schemes to capture correct long-time dynamics of the system. On the other hand, the unconditional stability of the energy dissipation preserving schemes provides flexibility for dealing with the stiffness issue in the model.

In this paper, we consider numerical approximations to the continuum MBE growth model (1.1) with free energy (1.2), which is obtained by minimizing the given free energy where the nonlinear potential is a fourth order Ginzburg–Landau double-well potential in terms of the gradient of a height function. Here we give a brief review of available papers in the literature on proposing efficient numerical schemes for solving the MBE model. In [46], Wang et al. used convex splitting strategy to propose unconditionally energy stable schemes for MBE model. Qiao et al. proposed an adaptive time-stepping strategy for the MBE model with slope selection [33], and Qiao et al. proposed energy stable schemes for the MBE model without slope selection and its convergence analysis [31]. Chen et al. proposed a linear energy stable scheme for MBE model without slope selection using convex splitting strategy [4]. In [28], Li et al. developed a spectral method for solving the MBE models. In [52], Xia proposed a full discrete stable scheme for MBE model without slope selection using discontinuous Galerkin method. Recently, Feng et al. developed a linearly preconditioned nonlinear conjugate gradient solver [8] and a second-order energy-stable BDF scheme for MBE model with slope selection [9]. Some other related papers include [19,22, 29,32,37].

Mainly, the strategies for developing energy stable schemes can be generally categorized into two parts. The first part named stabilized approach, where the nonlinear terms are treated explicitly, but some linear stabilizing terms are added to provide better stability of the scheme. This so-called stabilized approach have been broadly used in phase-field models, see [40,42–44,53,62,63,66,67]. Another approach is named “convex splitting”, which was originally proposed in [7] and has been exploited by the numerical analysis society [17,46,47,49,50]. The idea of convex splitting is to split the free energy as a convex potential minus another convex potential. Then the chemical potential from the first convex part is solved implicitly, and the rest is solved explicitly. The advantage of the stabilized approach is its simplicity to implement, as it is linear, but it is only first order in time (due to the first-order error introduced in the stabilizing term), and it has to assume/truncate the free energy (which should not be ignored in the continuum PDE level). For the convex splitting approach, its existence

and uniqueness of solution could be easily seen. However, the convex splitting scheme is usually nonlinear, which requires more computational cost. Besides, designing second-order convex splitting schemes is not trivial.

Recently, Yang and his collaborators have proposed a new approach named invariant energy quadratization (IEQ) to derive linearly unconditionally energy stable schemes for gradient flow models, which have energy-dissipation structure, see [54–60,64,65]. To name a few, in [60], IEQ is used to propose a linear and stable scheme for ternary phase field model; in [65], IEQ is used to propose a linear and stable scheme for the **Q**-tensor hydrodynamic model with Landau–DeGene free energy. The idea of IEQ was originated from [1], where the author named it "Lagrangian multiplier", as they are introducing intermediate variables to relax the norm of liquid crystal orientation vector into 1. Later [14,15] have extended this idea for Cahn–Hilliard or Allen–Cahn equations with double-well potentials. Yang and his collaborators later realized this idea of introducing intermediate variables could be extended to a more general case, and the essential idea of introducing this intermediate variable is to reformulate the free energy (Leyaponv functional) into a quadratic form. And this quadratization approach is rather general that a broad class PDE models which have the energy dissipation properties could be solved [54–60,64,65]. The IEQ idea has later been exploited to develop the SAV approach [38,39].

In our previous work [59], we have proposed first order and second order unconditionally energy stable schemes for MBE models (1.1) using the energy quadratization approach. In this paper, new schemes are proposed combining the IEQ and stabilization approaches. Mainly, IEQ is used to develop linear schemes, and the regularization parameter is introduced to make the proposed scheme more accurate and stable. We have shown that the newly proposed regularized schemes are second-order accurate in time, linear, unconditionally energy stable, and uniquely solvable.

The rest of the paper is organized as follows. In Section 2, we present the MBE model and its energy dissipation property. In Section 3, we develop the numerical schemes and prove their unconditional energy stability, unique solvability and error estimate in the semi-discretized case in time. In Section 4, we present some numerical simulations to demonstrate the accuracy and efficiency of the proposed schemes. Finally, some concluding remarks are presented in Section 5.

2. Molecular beam epitaxy model formulation

We consider the MBE model with slope selection, i.e. with the free energy in (1.2)

$$E(\phi) = \int_\Omega \Big(\frac{\varepsilon^2}{2}(\Delta\phi)^2 + \frac{1}{4}(|\nabla\phi|^2 - 1)^2\Big)d\Omega.$$

The chemical potential $\frac{\delta E}{\delta \phi}$ could be easily calculated as

$$\frac{\delta E}{\delta \phi} = \varepsilon^2\Delta^2\phi - \nabla\cdot((|\nabla\phi|^2 - 1)\nabla\phi). \tag{2.1}$$

After substituting (2.1) into the model (1.1), the governing equation for the Molecular Beam Epitaxial (MBE) model with slope selection is given by

$$\phi_t = -M\Big(\varepsilon^2\Delta^2\phi - \nabla\cdot((|\nabla\phi|^2 - 1)\nabla\phi)\Big), \tag{2.2}$$

where ϕ represents the epitaxy surface height, ε is a model parameter, and M is the mobility coefficient. With the periodic boundary condition or any other proper boundary condition that can satisfy the flux free condition at the boundary $\partial_{\mathbf{n}}\phi|_{\partial\Omega} = 0$ and $\partial_{\mathbf{n}}\Delta\phi|_{\partial\Omega} = 0$, we have the mass conservation property

$$\frac{d}{dt}\int_\Omega \phi(\mathbf{x}, t)d\Omega = 0, \tag{2.3}$$

where $\mathbf{n}$ is the outward normal on the boundary. And the model is thermodynamically consistent, in the sense that its energy is dissipative in time. As a matter of fact, we can calculate the energy dissipation rate

$$\frac{dE}{dt} = \int_\Omega \frac{\delta E}{\delta\phi}\frac{\delta\phi}{\delta t}d\Omega = -\int_\Omega M\Big(\varepsilon^2\Delta^2\phi - \nabla\cdot((|\nabla\phi|^2 - 1)\nabla\phi)\Big)^2 d\Omega, \tag{2.4}$$

with the expression of E as

$$E(\phi) = \int_\Omega \Big(\frac{\varepsilon^2}{2}(\Delta\phi)^2 + \frac{1}{4}(|\nabla\phi|^2 - 1)^2\Big)d\Omega. \tag{2.5}$$

Thus, one would like to propose discrete numerical schemes to preserve the properties: (1) mass conservation; (2) energy dissipation. And schemes preserving such properties are named energy stable scheme.

3. Numerical schemes

In this section, we first reformulate the MBE model by introducing an auxiliary variable and show the new form is equivalent to the original MBE model. Then we propose time discretization and spatial discretization subsequently to obtain linear and stable full discrete numerical approximations.

3.1. Equivalent form using energy quadratization approach

Recall the MBE model with slope selection reads

$$\phi_t = -M\Big(\varepsilon^2\Delta^2\phi - \nabla\cdot((|\nabla\phi|^2-1)\nabla\phi)\Big). \tag{3.1}$$

For simplicity, we consider periodic boundary condition. We introduce the auxiliary variable

$$q = |\nabla\phi|^2 - (1+\gamma), \tag{3.2}$$

with $\gamma > 0$ constant. Substituting (3.2) into (3.1), we have

$$\phi_t = -M\Big(\varepsilon^2\Delta^2\phi - \gamma\Delta\phi - \nabla\cdot(q\nabla\phi)\Big). \tag{3.3}$$

By taking derivative with respect to time for equation (3.2), we have

$$q_t = 2\nabla\phi\cdot\nabla\phi_t, \tag{3.4}$$

with $q|_{t=0} = \Big(|\nabla\phi| - (1+\gamma)\Big)|_{t=0}$. Therefore, if we combine equation (3.3) with equation (3.4), we obtain the equivalent model in a transformed expression:

$$\begin{cases} \phi_t = -M\Big[\varepsilon^2\Delta^2\phi - \gamma\Delta\phi - \nabla\cdot(q\nabla\phi)\Big], \\ q_t = 2\nabla\phi\cdot\nabla\phi_t, \end{cases} \tag{3.5}$$

with initial conditions

$$\begin{cases} \phi|_{t=0} = \phi_0, \\ q|_{t=0} = |\nabla\phi_0|^2 - (1+\gamma). \end{cases} \tag{3.6}$$

We remark that the transformed expression (3.5) is equivalent with the original model in primitive variables (3.1). And it could be easily seen that the transformed model (3.5) have the same property of mass conservation and energy dissipation. In particular, by substituting (3.2) into the expression of the energy, we have the energy and its dissipation rate in term of (ϕ, q):

$$\frac{dE(\phi,q)}{dt} = -\int_\Omega M\Big(\varepsilon^2\Delta\phi - \gamma\phi - \nabla\cdot(q\nabla\phi)\Big)^2 d\Omega, \tag{3.7}$$

where

$$E(\phi,q) = \int_\Omega \Big(\frac{\varepsilon^2}{2}(\Delta\phi)^2 + \frac{\gamma}{2}|\nabla\phi|^2 + \frac{1}{4}q^2 + \frac{1}{4}\big[1-(1+\gamma)^2\big]\Big)d\Omega. \tag{3.8}$$

The energy (3.8) and its dissipation rate (3.7) for the transformed model are equivalent with the original energy (2.5) and energy dissipation rate (2.4), by simply recognizing (3.2). Therefore, in the following sections, we will propose numerical approximation for the transformed model (3.5), and show the numerical schemes preserve the properties of mass conservation and energy dissipations, accordingly.

3.2. Time discretization

First of all, we will present the spatial discretization in this section. The energy stability and unique solvability will be presented as well. Here we propose three schemes: the first order Euler type, the second order Crank–Nicolson type, and the second order Adam–Bashforth type.

The first-order Euler scheme reads

Scheme 3.1. *Assuming that (ϕ^n, q^n) are already calculated with $n \geq 1$, we then compute (ϕ^{n+1}, q^{n+1}) from the following temporal discrete system:*

$$\frac{\phi^{n+1}-\phi^n}{\delta t} = -M\Big(\varepsilon^2\Delta^2\phi^{n+1} - \gamma\Delta\phi^{n+1} - \nabla\cdot(q^{n+1}\nabla\phi^n)\Big), \tag{3.9}$$

$$\frac{q^{n+1}-q^n}{\delta t} = 2\nabla\phi^n\cdot\nabla\frac{\phi^{n+1}-\phi^n}{\delta t}. \tag{3.10}$$

A second-order scheme based on Crank–Nicolson reads

Scheme 3.2. *Assuming that (ϕ^n, q^n), and (ϕ^{n-1}, q^{n-1}) are already calculated with $n \geq 1$, we then compute (ϕ^{n+1}, q^{n+1}) from the following temporal discrete system:*

$$\frac{\phi^{n+1}-\phi^n}{\delta t} = -M\Big(\varepsilon^2\Delta^2\phi^{n+\frac{1}{2}} - \gamma\Delta\phi^{n+\frac{1}{2}} - \nabla\cdot(q^{n+\frac{1}{2}}\nabla\overline{\phi}^{n+\frac{1}{2}})\Big), \tag{3.11}$$

$$\frac{q^{n+1}-q^n}{\delta t} = 2\nabla\overline{\phi}^{n+\frac{1}{2}}\cdot\nabla\frac{\phi^{n+1}-\phi^n}{\delta t}, \tag{3.12}$$

where $(\cdot)^{n+\frac{1}{2}} = \frac{1}{2}(\cdot)^n + (\cdot)^{n+1}$, $\overline{(\cdot)}^{n+\frac{1}{2}} = \frac{3}{2}(\cdot)^n - \frac{1}{2}(\cdot)^{n-1}$.

A second order Adam–Bashforth scheme:

Scheme 3.3. *Assuming that (ϕ^n, q^n), and (ϕ^{n-1}, q^{n-1}) are already calculated with $n \geq 1$, we then compute (ϕ^{n+1}, q^{n+1}) from the following temporal discrete system:*

$$\frac{3\phi^{n+1}-4\phi^n+\phi^{n-1}}{2\delta t} = -M\Big(\varepsilon^2\Delta^2\phi^{n+1} - \gamma\Delta\phi^{n+1} - \nabla\cdot(q^{n+1}\nabla\overline{\phi}^{n+1})\Big), \tag{3.13}$$

$$\frac{3q^{n+1}-4q^n+q^{n-1}}{2\delta t} = 2\nabla\overline{\phi}^{n+1}\cdot\nabla\frac{3\phi^{n+1}-4\phi^n+\phi^{n-1}}{2\delta t}, \tag{3.14}$$

where $\overline{(\cdot)}^{n+\frac{1}{2}} = 2(\cdot)^n - (\cdot)^{n-1}$.

Several remarks are summarized as follow.

Theorem 3.1. *The proposed schemes (3.9)–(3.10), (3.11)–(3.12) and (3.13)–(3.14) preserve the total mass.*

Proof. For the scheme (3.11)–(3.12), we take inner product of equation (3.11) with δt, we have

$$\int_\Omega \phi^{n+1}d\mathbf{x} - \int_\Omega \phi^n d\mathbf{x} = \delta t\int_\Omega -M\Big(\varepsilon^2\Delta^2\phi^{n+\frac{1}{2}} - \gamma\Delta\phi^{n+\frac{1}{2}} - \nabla\cdot(q^{n+\frac{1}{2}}\nabla\overline{\phi}^{n+\frac{1}{2}})\Big)d\mathbf{x} = 0. \tag{3.15}$$

Therefore,

$$\int_\Omega \phi^{n+1}d\mathbf{x} = \int_\Omega \phi^n d\mathbf{x}. \tag{3.16}$$

For the scheme (3.9)–(3.10) and (3.13)–(3.14), the proof is similar, we thus omit it. □

Remark 3.1. The Schemes 3.1, 3.2 and 3.3 are similar with the one proposed in [59]. But the novelty of our scheme is the introduction of regularization parameter γ, which we will show later that it improves the stability and accuracy significantly.

Remark 3.2. The Schemes 3.1, 3.2 and 3.3 are fully decoupled, i.e. at each time step, one can solve ϕ^{n+1} and q^{n+1} subsequently.

Theorem 3.2. *The scheme (3.9)–(3.10) satisfies the following energy dissipation law*

$$\tilde{E}^{n+1} + \delta t M\int_\Omega \Big(\varepsilon^2\Delta^2\phi^{n+1} - \gamma\Delta\phi^{n+1} - \nabla\cdot(q^{n+1}\nabla\phi^n)\Big)^2 d\mathbf{x} \leq \tilde{E}^n, \tag{3.17}$$

where

$$\tilde{E}^n(\phi^n, q^n) = \int_\Omega \Big(\frac{\varepsilon^2}{2}(\Delta\phi^n)^2 + \frac{\gamma}{2}|\nabla\phi^n|^2 + \frac{1}{4}(q^n)^2 + \frac{1}{4}\big[1-(1+\gamma)^2\big]\Big) d\mathbf{x}. \tag{3.18}$$

Proof. For the scheme (3.9)–(3.10), we take the L^2 inner product of (3.9) with $\delta t(\varepsilon^2\Delta^2\phi^{n+1} - \gamma\Delta\phi^{n+1} - \nabla\cdot(q^{n+1}\nabla\phi^n))$, we can obtain

$$\begin{aligned} &-\delta t M \int_\Omega \Big(\varepsilon^2\Delta^2\phi^{n+1} - \gamma\Delta\phi^{n+1} - \nabla\cdot(q^{n+1}\nabla\phi^n)\Big)^2 d\mathbf{x} \\ &= \Big((\phi^{n+1}-\phi^n), \varepsilon^2\Delta^2\phi^{n+1} - \gamma\Delta\phi^{n+1} - \nabla\cdot(q^{n+1}\nabla\phi^n)\Big). \end{aligned} \tag{3.19}$$

And then we take the L_2 inner product of (3.10) with $\frac{1}{2}q^{n+1}$, we can obtain

$$\frac{1}{2}(q^{n+1}-q^n, q^{n+1}) = (\nabla(\phi^{n+1}-\phi^n), q^{n+1}\nabla\phi^n) \tag{3.20}$$

Adding equations (3.19) and (3.20) will give us the result. □

Theorem 3.3. *The proposed scheme* (3.11)–(3.12) *satisfies the energy dissipation law*

$$E^{n+1} + \delta t M \int_\Omega \Big(\varepsilon^2\Delta^2\phi^{n+\frac{1}{2}} - \gamma\Delta\phi^{n+\frac{1}{2}} - \nabla\cdot(q^{n+\frac{1}{2}}\nabla\overline{\phi}^{n+\frac{1}{2}})\Big)^2 d\mathbf{x} = E^n, \tag{3.21}$$

where

$$E^n(\phi^n, q^n) = \int_\Omega \Big(\frac{\varepsilon^2}{2}(\Delta\phi^n)^2 + \frac{\gamma}{2}|\nabla\phi^n|^2 + \frac{1}{4}(q^n)^2 + \frac{1}{4}\big[1-(1+\gamma)^2\big]\Big) d\mathbf{x} \tag{3.22}$$

i.e. it is unconditionally energy stable.

Proof. As a matter of fact, for scheme (3.11)–(3.12), by taking the L_2 inner product of (3.11) with $\delta t(\varepsilon^2\Delta^2\phi^{n+\frac{1}{2}} - \gamma\Delta\phi^{n+\frac{1}{2}} - \nabla\cdot(q^{n+\frac{1}{2}}\nabla\overline{\phi}^{n+\frac{1}{2}}))$, we will have

$$\begin{aligned} &-\delta t M \int_\Omega \Big(\varepsilon^2\Delta^2\phi^{n+\frac{1}{2}} - \gamma\Delta\phi^{n+\frac{1}{2}} - \nabla\cdot(q^{n+\frac{1}{2}}\nabla\overline{\phi}^{n+\frac{1}{2}})\Big)^2 d\mathbf{x} \\ &= \Big(\phi^{n+1}-\phi^n, (\varepsilon^2\Delta^2\phi^{n+\frac{1}{2}} - \gamma\Delta\phi^{n+\frac{1}{2}} - \nabla\cdot(q^{n+\frac{1}{2}}\nabla\overline{\phi}^{n+\frac{1}{2}}))\Big) \\ &= \frac{\varepsilon^2}{2}(|\Delta\phi^{n+1}|^2 - |\Delta\phi^n|^2) + \frac{\gamma}{2}(|\nabla\phi^{n+1}|^2 - |\nabla\phi^n|^2) + (\nabla(\phi^{n+1}-\phi^n), q^{n+\frac{1}{2}}\nabla\overline{\phi}^{n+\frac{1}{2}}). \end{aligned} \tag{3.23}$$

Then by taking L_2 inner product of (3.12) with $\frac{1}{2}\delta t q^{n+\frac{1}{2}}$ with (3.12), then integrating by parts, we have

$$\frac{1}{4}((q^{n+1})^2 - (q^n)^2, 1) = (\nabla(\phi^{n+1}-\phi^n), q^{n+\frac{1}{2}}\nabla\overline{\phi}^{n+\frac{1}{2}}). \tag{3.24}$$

Adding equations (3.23) and (3.24), we obtain

$$E^{n+1} + \delta t M \int_\Omega \Big(\varepsilon^2\Delta^2\phi^{n+\frac{1}{2}} - \gamma\Delta\phi^{n+\frac{1}{2}} - \nabla\cdot(q^{n+\frac{1}{2}}\nabla\overline{\phi}^{n+\frac{1}{2}})\Big)^2 d\mathbf{x} = E^n, \tag{3.25}$$

where $E^n(\phi^n, q^n) = \int_\Omega \Big(\frac{\varepsilon^2}{2}(\Delta\phi^n)^2 + \frac{\gamma}{2}|\nabla\phi^n|^2 + \frac{1}{4}(q^n)^2 + \frac{1}{4}\big[1-(1+\gamma)^2\big]\Big) d\mathbf{x}$. This closes the proof. □

Theorem 3.4. *The scheme* (3.13)–(3.14) *satisfies the following energy dissipation law*

$$\tilde{E}^{n+1} + \delta t M \int_\Omega \Big(\varepsilon^2\Delta^2\phi^{n+1} - \gamma\Delta\phi^{n+1} - \nabla\cdot(q^{n+1}\nabla\overline{\phi}^{n+\frac{1}{2}})\Big)^2 d\mathbf{x} \le \tilde{E}^n, \tag{3.26}$$

where

$$\tilde{E}^n(\phi^n, q^n) = \int_\Omega \Big(\frac{\varepsilon^2}{4}((\Delta\phi^n)^2 + (\Delta(2\phi^n - \phi^{n-1}))^2) + \frac{\gamma}{4}\Big(|\nabla\phi^n|^2 + |\nabla(2\phi^n - \phi^{n-1})^2\Big) + \frac{1}{8}\Big((q^n)^2 + (2q^n - q^{n-1})^2) + \frac{1}{4}\big[1 - (1+\gamma)^2\big]\Big)d\mathbf{x}. \tag{3.27}$$

Proof. The proof is similar, we thus only show the sketch. By the same manner, for the scheme (3.13)–(3.14), we take the L^2 inner product of (3.13) with $\delta t(\varepsilon^2\Delta^2\phi^{n+1} - \gamma\Delta\phi^{n+1} - \nabla\cdot(q^{n+1}\nabla\overline{\phi}^{n+\frac{1}{2}}))$, we can obtain

$$\begin{aligned} &-\delta t M \int_\Omega \Big(\varepsilon^2\Delta^2\phi^{n+1} - \gamma\Delta\phi^{n+1} - \nabla\cdot(q^{n+1}\nabla\overline{\phi}^{n+\frac{1}{2}})\Big)^2 d\mathbf{x} \\ =&\Big(\frac{1}{2}(3\phi^{n+1} - 4\phi^n + \phi^{n-1}), \varepsilon^2\Delta^2\phi^{n+1} - \gamma\Delta\phi^{n+1} - \nabla\cdot(q^{n+1}\nabla\overline{\phi}^{n+\frac{1}{2}})\Big). \end{aligned} \tag{3.28}$$

And then we take the L_2 inner product of (3.14) with $\frac{1}{2}q^{n+1}$, we can obtain

$$(\frac{1}{2}(3q^{n+1} - 4q^n + q^{n-1}, q^{n+1})) = (\nabla(3\phi^{n+1} - 4\phi^n + \phi^{n-1}, q^{n+1}\nabla\overline{\phi}^{n+1}). \tag{3.29}$$

Adding equations (3.28) and (3.29) will give us the result. □

Theorem 3.5. *The proposed schemes* (3.9)–(3.10), (3.11)–(3.12) *and* (3.13)–(3.14) *are uniquely solvable.*

Proof. First of all, let us look at the scheme (3.9)–(3.10), from (3.10), we have

$$q^{n+1} = q^n + \nabla\phi^n\cdot\nabla(\phi^{n+1} - \phi^n). \tag{3.30}$$

Replacing q^{n+1} in (3.9), then the scheme (3.9)–(3.10) is equal to

- Step 1: update ϕ^{n+1} via

$$\mathcal{T}\phi^{n+1} = f(\phi^n, \phi^{n-1}), \tag{3.31}$$

where the linear operator is

$$\mathcal{T}\phi = \frac{\phi}{\delta t} + M\varepsilon^2\Delta^2\phi - M\gamma\Delta\phi - \nabla\cdot(\nabla\phi^n\cdot\nabla\phi)\nabla\phi^n, \tag{3.32}$$

and the right-hand-side is

$$f = \frac{\phi^n}{\delta t} - M\nabla\cdot(\nabla\phi^n\cdot\nabla\phi^n\nabla\phi^n) + M\nabla\cdot(q^n\nabla\phi^n). \tag{3.33}$$

- Step 2: update q^{n+1} via

$$q^{n+1} = q^n + 2\nabla\phi^n\cdot\nabla(\phi^{n+1} - \phi^n). \tag{3.34}$$

By the Lax–Milgram theorem, there exists a unique solution for (3.31). Thus the scheme (3.9)–(3.10) is uniquely solvable.

Then we consider the scheme (3.11)–(3.12). As a matter of fact, in scheme (3.11)–(3.12), ϕ^{n+1} and q^{n+1} could be decoupled, i.e. we solve ϕ^{n+1} first and then update q^{n+1} sequentially.

In details, from (3.12), we have

$$q^{n+\frac{1}{2}} = q^n + \nabla\overline{\phi}^{n+\frac{1}{2}}\cdot\nabla(\phi^{n+1} - \phi^n). \tag{3.35}$$

Replacing $q^{n+\frac{1}{2}}$ in (3.11), then the scheme (3.11)–(3.12) is equal to

- Step 1: update ϕ^{n+1} via

$$\mathcal{T}\phi^{n+1} = f(\phi^n, \phi^{n-1}), \tag{3.36}$$

where the linear operator is

$$\mathcal{T}\phi = \frac{\phi}{\delta t} + \frac{M\varepsilon^2}{2}\Delta^2\phi - \frac{M\gamma}{2}\Delta\phi - \nabla\cdot(\nabla\overline{\phi}^{n+\frac{1}{2}}\cdot\nabla\phi)\nabla\overline{\phi}^{n+\frac{1}{2}}, \tag{3.37}$$

and the right-hand-side is

$$f = \frac{\phi^n}{\delta t} - M\nabla\cdot(\nabla\overline{\phi}^{n+\frac{1}{2}}\cdot\nabla\phi^n\nabla\overline{\phi}^{n+\frac{1}{2}}) + M\nabla\cdot(q^n\nabla\overline{\phi}^{n+\frac{1}{2}}) + \frac{M\varepsilon^2}{2}\Delta^2\phi^n - \frac{M\gamma}{2}\Delta\phi^n. \tag{3.38}$$

- Step 2: update q^{n+1} via

$$q^{n+1} = q^n + 2\nabla\overline{\phi}^{n+\frac{1}{2}}\cdot\nabla(\phi^{n+1}-\phi^n). \tag{3.39}$$

It could be easily shown that there exists a unique solution for (3.36) using the Lax–Milgram theorem. Thus the scheme (3.11)–(3.12) is uniquely solvable.

In a similar manner, for the scheme (3.13)–(3.14), we can reformulate it into a decoupled scheme by substituting q^{n+1} of (3.14) into (3.13). In details, from (3.14), we have

$$q^{n+1} = \frac{4}{3}q^n - \frac{1}{3}q^{n-1} + 2\nabla\overline{\phi}^{n+\frac{1}{2}}\cdot\nabla(\phi^{n+1} - \frac{4}{3}\phi^n + \frac{1}{3}\phi^{n-1}). \tag{3.40}$$

Then substituting the expression of q^{n+1} into equation (3.13), we have the scheme

- Step 1: update ϕ^{n+1} via

$$\mathcal{T}\phi^{n+1} = f(\phi^n, \phi^{n-1}), \tag{3.41}$$

where the linear operator is

$$\mathcal{T}\phi = \frac{3}{2\delta t}\phi + M\varepsilon^2\Delta^2\phi - M\gamma\Delta\phi - M\nabla\cdot(2\nabla\overline{\phi}^{n+1}\cdot\nabla\phi^{n+1}\nabla\overline{\phi}^{n+1}), \tag{3.42}$$

and the right-hand-side is

$$f = \frac{4\phi^n - \phi^{n-1}}{2\delta t} + M\cdot(\frac{4q^n}{3} - \frac{q^{n-1}}{3} + 2\nabla\overline{\phi}^{n+1}\cdot\nabla(\phi^{n+1} - \frac{4\phi^n}{3} + \frac{\phi^{n-1}}{3})\nabla\overline{\phi}^{n+1}). \tag{3.43}$$

- Step 2: update q^{n+1} via

$$q^{n+1} = \frac{4}{3}q^n - \frac{1}{3}q^{n-1} + 2\nabla\overline{\phi}^{n+1}\cdot\nabla(\phi^{n+1} - \frac{4}{3}\phi^n + \frac{1}{3}\phi^{n-1}). \tag{3.44}$$

Similarly, the scheme (3.41) could be easily shown to exist a unique solution by Lax–Milgram theory. Then, the scheme (3.13)–(3.14) is uniquely solvable. □

Remark 3.3. The difference of the regularized schemes compared with the schemes in [59] lies in the extra term in the linear operator, i.e., $-\frac{M\gamma}{2}\Delta\phi$ of equation (3.37) in the CN scheme, and $-M\gamma\Delta\phi$ of equation (3.32) and (3.42) in the BDF scheme. These two terms would regularize the linear operator. Thus we name this strategy regularized IEQ approach.

3.3. Error analysis

To simplify the notations, without loss of generality, in the below, we let $M = \varepsilon = 1$. We use $x \lesssim y$ to denote there exists a constant C that is independent of δt and n such that $x \le Cy$. We let $L^p(\Omega)$ denote the usual Lebesgue space on Ω with the norm $\|\cdot\|_{L^p}$. The inner product and norm in $L^2(\Omega)$ are denoted by $(\cdot,\cdot)$ and $\|\cdot\|$, respectively. $W^{k,p}(\Omega)$ stands for the standard Sobolev spaces equipped with the standard Sobolev norms $\|\cdot\|_{k,p}$. For $p = 2$, we write $H^k(\Omega)$ for $W^{k,2}(\Omega)$, and the corresponding norm is $\|\cdot\|_k$.

We now focus on the error estimates for the first order scheme (3.9)–(3.10). We formulate the PDE system (3.5) as a truncation form:

$$\frac{\phi(t_{n+1}) - \phi(t_n)}{\delta t} = -(\Delta^2\phi(t_{n+1}) - \gamma\Delta\phi(t_{n+1}) - \nabla\cdot(q(t_{n+1})\nabla\phi(t_n)) + R_\phi^{n+1}, \tag{3.45}$$

$$q(t_{n+1}) - q(t_n) = 2\nabla\phi(t_n)\cdot\nabla(\phi(t_{n+1}) - \phi(t_n)) + \delta t R_q^{n+1}, \tag{3.46}$$

where

$$\begin{cases} R_\phi^{n+1} = \dfrac{\phi(t_{n+1}) - \phi(t_n)}{\delta t} - \phi_t(t_{n+1}) + \nabla\cdot(q(t_{n+1})\nabla\phi(t_n)) - \nabla\cdot(q(t_{n+1})\nabla\phi(t_{n+1})), \\ R_q^{n+1} = \dfrac{q(t_{n+1}) - q(t_n)}{\delta t} - q_t(t_{n+1}) + 2\nabla\phi(t_{n+1})\cdot\nabla\phi_t(t_{n+1}) - 2\nabla(\phi(t_n))\cdot\nabla(\dfrac{\phi(t_{n+1}) - \phi(t_n)}{\delta t}). \end{cases} \tag{3.47}$$

We assume the exact solution ϕ, q of the system (3.5) possesses the following regularity conditions,

$$\begin{cases} \phi \in L^\infty(0,T;H^2(\Omega)), q \in L^\infty(0,T;W^{1,\infty}(\Omega)), \\ \phi_t \in L^2(0,T;L^2(\Omega)) \cap L^\infty(0,T;H^2(\Omega)), \phi_{tt}, q_{tt} \in L^2(0,T;L^2(\Omega)). \end{cases} \tag{3.48}$$

One can easily establish the following estimates for the truncation errors, provided that the exact solutions of the system (3.5) satisfy the regularity conditions (3.48).

Lemma 3.1. *Under the regularity conditions (3.48), the truncation errors satisfy*

$$\delta t \sum_{n=0}^{[\frac{T}{\delta t}]} (\|R_\phi^{n+1}\|^2 + \|R_q^{n+1}\|^2) \lesssim \delta t^2. \tag{3.49}$$

Since the proof for Lemma 3.1 is rather straightforward, we leave this to the interested readers.
To derive the error estimates, we denote the error functions as

$$e_\phi^n = \phi(t_n) - \phi^n, e_q^n = q(t_n) - q^n. \tag{3.50}$$

By subtracting (3.45)–(3.46) from (3.9)–(3.10), we derive the error equations:

$$\frac{e_\phi^{n+1} - e_\phi^n}{\delta t} + \Delta^2 e_\phi^{n+1} - \gamma \Delta e_\phi^{n+1} - \nabla \cdot (\nabla e_\phi^n q(t_{n+1}) - \nabla e_\phi^n e_q^{n+1} + \nabla \phi(t_n) e_q^{n+1}) = R_\phi^{n+1}, \tag{3.51}$$

$$e_q^{n+1} - e_q^n = 2(\nabla \phi(t_n) \cdot \nabla (e_\phi^{n+1} - e_\phi^n) - \nabla e_\phi^n \cdot \nabla (e_\phi^{n+1} - e_\phi^n) + \nabla e_\phi^n \cdot \nabla (\phi(t_{n+1}) - \phi(t_n))) + \delta t R_q^{n+1}. \tag{3.52}$$

Theorem 3.6. *Under the regularity conditions of (3.48), for $0 \le m \le [\frac{T}{\delta t}] - 1$, it holds*

$$\|\Delta e_\phi^{m+1}\|^2 + \gamma \|\nabla e_\phi^{m+1}\|^2 + \|e_q^{m+1}\|^2 \lesssim \delta t^2. \tag{3.53}$$

Proof. By taking the L^2 inner product of (3.51) with $e_\phi^{n+1} - e_\phi^n$, we obtain

$$\begin{aligned} &\frac{1}{\delta t}\|e_\phi^{n+1} - e_\phi^n\|^2 + \frac{1}{2}\Big(\|\Delta e_\phi^{n+1}\|^2 - \|\Delta e_\phi^n\|^2 + \|\Delta e_\phi^{n+1} - \Delta e_\phi^n\|^2\Big) \\ &\quad + \frac{\gamma}{2}\Big(\|\nabla e_\phi^{n+1}\|^2 - \|\nabla e_\phi^n\|^2 + \|\nabla e_\phi^{n+1} - \nabla e_\phi^n\|^2\Big) \\ &\quad = (R_\phi^{n+1}, e_\phi^{n+1} - e_\phi^n) - (\nabla e_\phi^n q(t_{n+1}), \nabla e_\phi^{n+1} - \nabla e_\phi^n) \\ &\qquad + (\nabla e_\phi^n e_q^{n+1}, \nabla e_\phi^{n+1} - \nabla e_\phi^n) \\ &\qquad - (\nabla \phi(t_n) e_q^{n+1}, \nabla e_\phi^{n+1} - \nabla e_\phi^n). \end{aligned} \tag{3.54}$$

By taking the L^2 inner product of (3.52) with $\frac{1}{2}e_q^{n+1}$, we obtain

$$\begin{aligned} &\tfrac{1}{4}(\|e_q^{n+1}\|^2 - \|e_q^n\|^2 + \|e_q^{n+1} - e_q^n\|^2) = \tfrac{1}{2}\delta t (R_q^{n+1}, e_q^{n+1}) + (\nabla e_\phi^n \cdot \nabla(\phi(t_{n+1}) - \phi(t_n)), e_q^{n+1}) \\ &\quad - (\nabla e_\phi^n \cdot \nabla (e_\phi^{n+1} - e_\phi^n), e_q^{n+1}) + (\nabla \phi(t_n) \cdot \nabla (e_\phi^{n+1} - e_\phi^n), e_q^{n+1}). \end{aligned} \tag{3.55}$$

By combining (3.54) and (3.55) and multiplying with δt, we obtain

$$\begin{aligned} &\|e_\phi^{n+1} - e_\phi^n\|^2 + \frac{\delta t}{2}\Big(\|\Delta e_\phi^{n+1}\|^2 - \|\Delta e_\phi^n\|^2 + \|\Delta e_\phi^{n+1} - \Delta e_\phi^n\|^2\Big) \\ &\quad + \frac{\gamma \delta t}{2}\Big(\|\nabla e_\phi^{n+1}\|^2 - \|\nabla e_\phi^n\|^2 + \|\nabla e_\phi^{n+1} - \nabla e_\phi^n\|^2\Big) \\ &\quad + \frac{\delta t}{4}(\|e_q^{n+1}\|^2 - \|e_q^n\|^2 + \|e_q^{n+1} - e_q^n\|^2) \\ &\quad = -\delta t (\nabla e_\phi^n q(t_{n+1}), \nabla e_\phi^{n+1} - \nabla e_\phi^n) \\ &\qquad + \delta t (\nabla e_\phi^n \cdot \nabla(\phi(t_{n+1}) - \phi(t_n)), e_q^{n+1}) \\ &\qquad + \delta t (R_\phi^{n+1}, e_\phi^{n+1} - e_\phi^n) \\ &\qquad + \frac{1}{2}\delta t^2 (R_q^{n+1}, e_q^{n+1}). \end{aligned} \tag{3.56}$$

We estimate the terms on the right hand side one by one as follows.

$$\begin{aligned}\delta t|(\nabla e_\phi^n q(t_{n+1}), \nabla e_\phi^{n+1} - \nabla e_\phi^n)| &\le \delta t|(\Delta e_\phi^n q(t_{n+1}), e_\phi^{n+1} - e_\phi^n)| + \delta t|(\nabla e_\phi^n \cdot \nabla q(t_{n+1}), e_\phi^{n+1} - e_\phi^n)| \\ &\lesssim \delta t^2\|\Delta e_\phi^n\|^2 + \delta t^2\|\nabla e_\phi^n\|^2 + \frac{1}{2}\|e_\phi^{n+1} - e_\phi^n\|^2;\end{aligned} \tag{3.57}$$

$$\begin{aligned}\delta t|(\nabla e_\phi^n \cdot \nabla(\phi(t_{n+1}) - \phi(t_n)), e_q^{n+1})| &\lesssim \delta t\|\nabla e_\phi^n\|_{L^4}\|\nabla(\phi(t_{n+1}) - \phi(t_n))\|_{L^4}\|e_q^{n+1}\| \\ &\lesssim \delta t^2\|\Delta e_\phi^n\|\|e_q^{n+1}\| \\ &\lesssim \delta t^2\|\Delta e_\phi^n\|^2 + \delta t^2\|e_q^{n+1}\|^2;\end{aligned} \tag{3.58}$$

$$\delta t|(R_\phi^{n+1}, e_\phi^{n+1} - e_\phi^n)| \lesssim \frac{1}{2}\|e_\phi^{n+1} - e_\phi^n\|^2 + \delta t^2\|R_\phi^{n+1}\|^2; \tag{3.59}$$

$$\frac{1}{2}\delta t^2(R_q^{n+1}, e_q^{n+1}) \lesssim \delta t^2\|R_q^{n+1}\|^2 + \delta t^2\|e_q^{n+1}\|^2. \tag{3.60}$$

By combining the above estimates with (3.56), we obtain

$$\begin{aligned}&\frac{1}{2}\Big(\|\Delta e_\phi^{n+1}\|^2 - \|\Delta e_\phi^n\|^2 + \|\Delta e_\phi^{n+1} - \Delta e_\phi^n\|^2\Big) \\ &\quad + \frac{\gamma}{2}\Big(\|\nabla e_\phi^{n+1}\|^2 - \|\nabla e_\phi^n\|^2 + \|\nabla e_\phi^{n+1} - \nabla e_\phi^n\|^2\Big) \\ &\quad + \frac{1}{4}(\|e_q^{n+1}\|^2 - \|e_q^n\|^2 + \|e_q^{n+1} - e_q^n\|^2) \\ &\quad \lesssim \delta t\|\Delta e_\phi^n\|^2 + \delta t\|\nabla e_\phi^n\|^2 + \delta t\|e_q^{n+1}\|^2 + \delta t\|R_\phi^{n+1}\|^2 + \delta t\|R_q^{n+1}\|^2.\end{aligned} \tag{3.61}$$

Summing up the above inequality from $n = 0$ to $m \le [\frac{T}{\delta t}] - 1$, using Lemma 3.1 and dropping some unnecessary terms, we obtain

$$\|\Delta e_\phi^{m+1}\|^2 + \gamma\|\nabla e_\phi^{m+1}\|^2 + \|e_q^{m+1}\|^2 \lesssim \delta t\sum_{n=0}^{m}(\|\Delta e_\phi^{n+1}\|^2 + \gamma\|\nabla e_\phi^{n+1}\|^2 + \|e_q^{n+1}\|^2) + \delta t^2. \tag{3.62}$$

By applying the discrete Gronwall Lemma to the above inequality, we have

$$\|\Delta e_\phi^{m+1}\|^2 + \gamma\|\nabla e_\phi^{m+1}\|^2 + \|e_q^{m+1}\|^2 \lesssim \delta t^2, \tag{3.63}$$

which concludes the theorem. □

The error estimates for the second order schemes, as well as the fully discrete schemes in the context of finite element method or spectral method, can be derived in a similar way, see [2,6,10,11,18,34,35,41,48,51,61].

3.4. Spatial discretization using spectral methods

Fourier spectral method is employed to handle the spatial discretization, since it is one of the most suitable spatial approximation methods for periodic problems. We use the following Fourier basis functions:

$$\mathbb{P}_M = span\{1, \sin nx, \cos nx, n = 1, 2, \ldots, N\} \times span\{1, \sin my, \cos my, m = 1, 2, \ldots, M\}, \tag{3.64}$$

where N is the number of the Fourier mode.

Then the weak formulation of scheme (3.1) can be written as follows:

Scheme 3.4. *Give the initial condition*

$$\begin{cases}\phi_N^0 = \phi_0, \\ q_N^0 = |\nabla\phi_0|^2 - (1+\gamma).\end{cases} \tag{3.65}$$

After calculated (ϕ_N^n, q_N^n)*, find* $\phi_N^{n+1} \in \mathbb{P}_M$ *such that*

$$\begin{aligned}&\Big(\frac{\phi_N^{n+1} - \phi_N^n}{\delta t}, \varphi_N\Big) = -M\Big(\varepsilon^2\Delta^2\phi_N^{n+1} - \gamma\Delta\phi_N^{n+1} - \nabla\cdot(q_N^{n+1}\nabla\phi_N^n), \varphi_N\Big), \forall\varphi_N \in \mathbb{P}_M, \\ &\Big(\frac{q_N^{n+1} - q_N^n}{\delta t}, \psi_N\Big) = \Big(2\nabla\phi_N^{n+1}\cdot\nabla\frac{\phi_N^{n+1} - \phi_N^n}{\delta t}, \psi_N\Big), \forall\psi_N \in \mathbb{P}_M.\end{aligned} \tag{3.66}$$

And the weak formulation of scheme (3.2) can be written as follows:

Scheme 3.5. *Give the initial condition*

$$\begin{cases} \phi_N^0 = \phi_0, \\ q_N^0 = |\nabla \phi_0|^2 - (1+\gamma). \end{cases} \tag{3.67}$$

After calculated (ϕ_N^n, q_N^n) *and* $(\phi_N^{n-1}, q_N^{n-1})$, *find* $\phi_N^{n+1} \in \mathbb{P}_M$ *such that*

$$\begin{aligned} &\Big(\frac{\phi_N^{n+1} - \phi_N^n}{\delta t}, \varphi_N\Big) = -M\Big(\varepsilon^2 \Delta^2 \phi_N^{n+\frac{1}{2}} - \gamma \Delta \phi_N^{n+\frac{1}{2}} - \nabla \cdot (q_N^{n+\frac{1}{2}} \nabla \overline{\phi}_N^{n+\frac{1}{2}}), \varphi_N\Big), \forall \varphi_N \in \mathbb{P}_M, \\ &\Big(\frac{q_N^{n+1} - q_N^n}{\delta t}, \psi_N\Big) = \Big(2\nabla \overline{\phi}_N^{n+\frac{1}{2}} \cdot \nabla \frac{\phi_N^{n+1} - \phi_N^n}{\delta t}, \psi_N\Big), \forall \psi_N \in \mathbb{P}_M. \end{aligned} \tag{3.68}$$

Similarly, the weak formulation of scheme (3.3) can be written as follows:

Scheme 3.6. *Give the initial condition*

$$\begin{cases} \phi_N^0 = \phi_0, \\ q_N^0 = |\nabla \phi_0|^2 - (1+\gamma). \end{cases} \tag{3.69}$$

After calculating (ϕ_N^n, q_N^n) *and* $(\phi_N^{n-1}, q_N^{n-1})$, *find* $\phi_N^{n+1} \in \mathbb{P}_M$ *such that*

$$\begin{aligned} &\Big(\frac{3\phi_N^{n+1} - 4\phi_N^n + \phi_N^{n-1}}{2\delta t}, \varphi_N\Big) = -M\Big(\varepsilon^2 \Delta^2 \phi_N^{n+1} - \gamma \Delta \phi_N^{n+1} - \nabla \cdot (q_N^{n+1} \nabla \overline{\phi}_N^{n+1}), \varphi_N\Big), \forall \varphi_N \in \mathbb{P}_M, \\ &\Big(\frac{3q_N^{n+1} - 4q_N^n + q_N^{n-1}}{2\delta t}, \psi_N\Big) = \Big(2\nabla \overline{\phi}_N^{n+1} \cdot \nabla \frac{3\phi_N^{n+1} - 4\phi_N^n + \phi_N^{n-1}}{2\delta t}, \psi_N\Big), \forall \psi_N \in \mathbb{P}_M. \end{aligned} \tag{3.70}$$

It could be easily shown that the full discrete linear scheme is uniquely solvable, and it also preserves the mass conservation and energy dissipation properties in the full discrete sense. The proves are similar. We thus omit them for simplicity.

4. Numerical results

In this section, we will give several numerical simulations of the MBE model by the two schemes: Scheme 3.5 and Scheme 3.6, i.e. equations (3.68) and (3.70). Also the efficiency and accuracy of the proposed numerical schemes by adding the regularization parameter γ will be demonstrated. In the rest of the paper, we chose periodic boundary conditions in the square domain $[0, L]^2$, and employ the second order schemes since the second order schemes are more accurate.

4.1. Convergence rate test

First of all, consider MBE model (2.2) with the initial condition as follows:

$$\phi(x, y, t = 0) = 0.1(\sin 3x \sin 2y + \sin 5x \sin 5y). \tag{4.1}$$

The computational domain is $[0, 2\pi]^2$. The space is discretize by 128×128 grid points by the Fourier spectral method.

Define the roughness measure function $W(t)$ as follows:

$$W(t) = \sqrt{\frac{1}{|\Omega|} \int_\Omega \Big(\phi(x, y, t) - \overline{\phi}(x, y, t)\Big)^2 d\Omega}, \tag{4.2}$$

where $\overline{\phi}(x, y, t) = \int_\Omega \phi(x, y, t) d\Omega$. We begin with time accuracy for the two schemes (3.68) and (3.70). We use numerical results of scheme (3.68) with $\gamma = 0, \delta t = 0.00001$ and $N = 512$ as the exact solution since the exact solution for MBE growth model is unknown. Taking $\varepsilon = 1$ and the numerical errors are computed at $t = 1$. Fig. 4.1 shows the L^2-errors versus time step δt for the MBE growth model using second order Adam–Bashforth scheme (3.70) (left) and Crank–Nicolson scheme (3.68) (right). With different regularization parameter $\gamma = 0, 1$, the expected second order convergence rate in time is obtained.

From Fig. 4.1, we observe the two schemes, i.e. Adam–Bashforth scheme (3.70) and Crank–Nicolson scheme (3.68) provide similar accuracy/error. In the later discussion, we thus only use Crank–Nicolson scheme (3.68) without loss of generality.

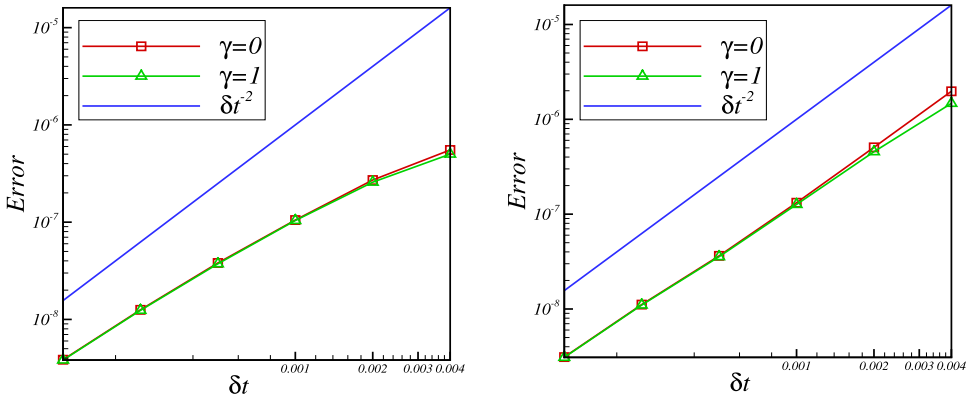

Fig. 4.1. Time accuracy convergence test. In the figures, the error versus time step δt for the MBE growth model are shown using second order Adam–Bashforth scheme (3.70) (left) and Crank–Nicolson scheme (3.68), with $\varepsilon^2 = 1$ and different regularization parameter $\gamma = 0, 1$.

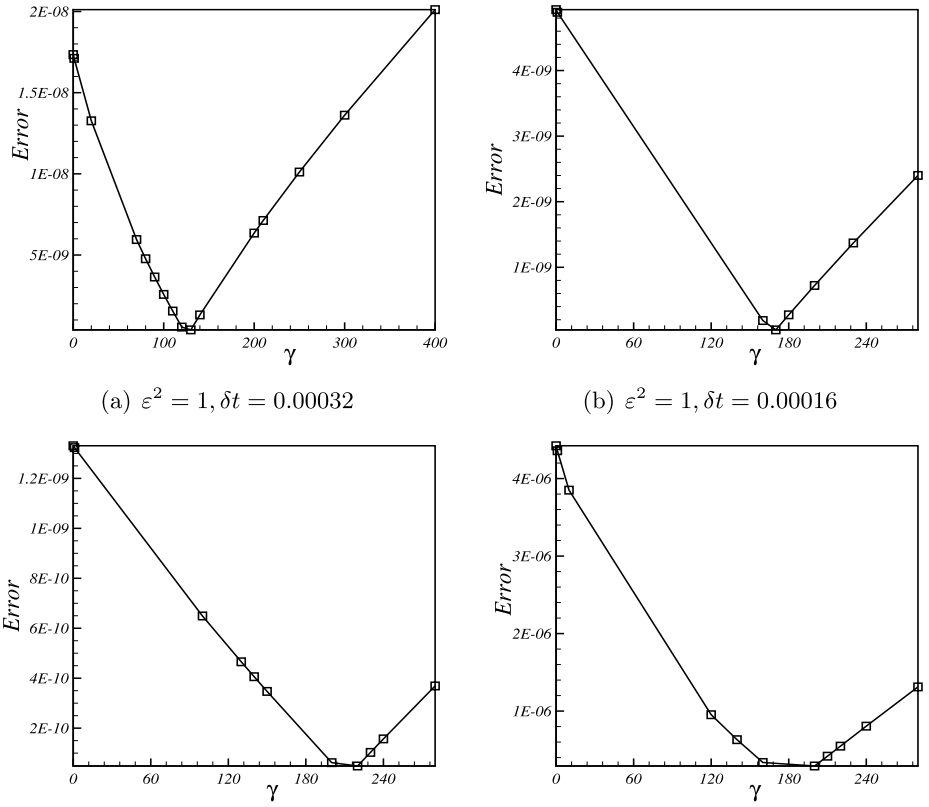

(a) $\varepsilon^2 = 1, \delta t = 0.00032$ (b) $\varepsilon^2 = 1, \delta t = 0.00016$

(c) $\varepsilon^2 = 1, \delta t = 0.00008$ (d) $\varepsilon^2 = 0.1, \delta t = 0.00032$

Fig. 4.2. The error of numerical solution ϕ_N versus γ using scheme (3.68) with different δt and ε.

4.2. Choices of the regularization parameter γ

Then, in this section, we investigate the choice of the regularization parameter γ that would provide better stability and accuracy. Fig. 4.2 plots the error of numerical solution ϕ_N versus γ using scheme (3.68) with different δt and ε. It shows that for a fixed δt and ε, the error decreasing as increasing γ, but it reaches the minimum then it increases as γ increases. In anther word, there exist some choices of regularization parameter γ such that the scheme is more stable and accurate. However, the optimal choice of γ is not known theoretically. In particular, we can easily observe $\gamma = 0$ (i.e. the scheme proposed in [59]) is not optimal.

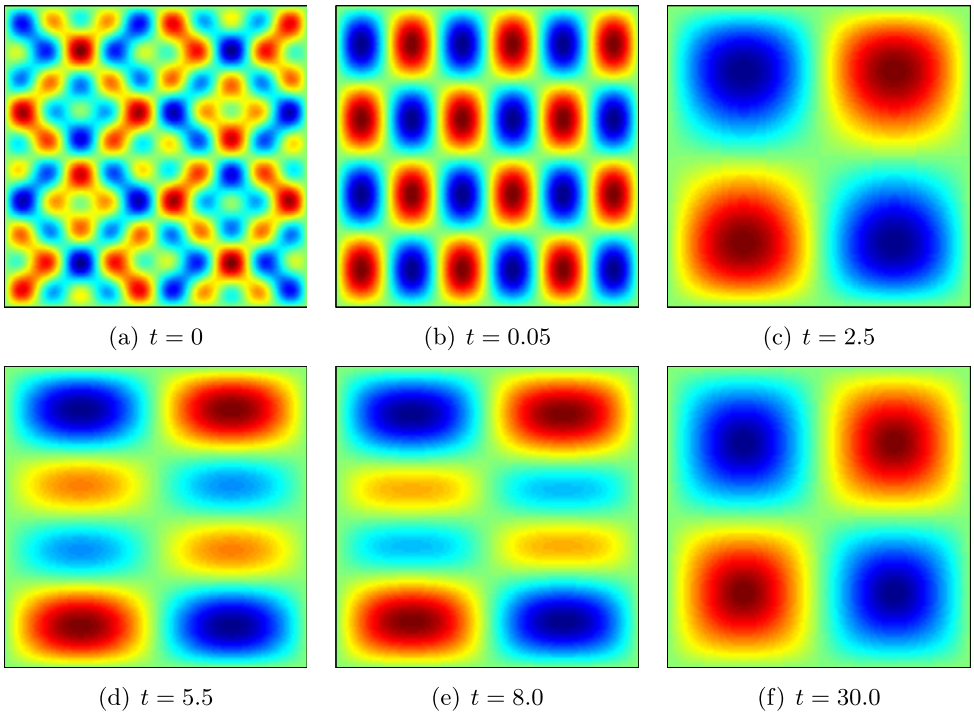

Fig. 4.3. The isolines of numerical solutions of the height function ϕ for the MBE growth model using Crank–Nicolson scheme (3.2). With $\varepsilon^2 = 0.1$, $\gamma = 20$ and time step $\delta t = 0.001$. Snapshots are taken at $t = 0, 0.05, 2.5, 5.5, 8, 30$, respectively.

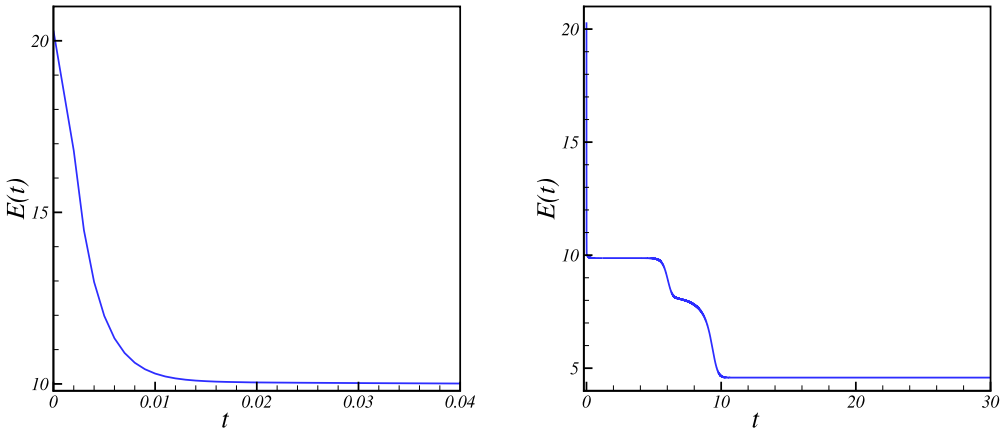

Fig. 4.4. Time evolution of the energy for the MBE growth model using Crank–Nicolson scheme (3.2) when $t \in [0, 30]$. The time step is set at $\delta t = 10^{-3}$ and $\gamma = 20$.

In Fig. 4.3, we show the contour lines of the numerical solutions ϕ up to the steady state ($t = 30$) by the Crank–Nicolson scheme (3.68). The evolution of energy curves and the roughness are plotted in Fig. 4.4 and Fig. 4.5 respectively. These computational results quite agree with the published results in [59].

In the meanwhile, we give the time evolution of the energy when $t \in [0, 15]$ with different time step δt and regularization parameter γ, shown in Fig. 4.6. Also, we enlarge time evolution of the energy with different time step and γ at time region $[0, 0.012]$ (left) and $[4, 12]$ (right) respectively (shown in Fig. 4.7), since the energy are decaying rapidly between this two time intervals. From Fig. 4.6 and Fig. 4.7, we observe the energy evolution is very close to the exact one with time step $\delta t = 10^{-4}$, and $\delta t = 10^{-3}$ by adding regularization parameter $\gamma = 20.0$. But the results with $\delta t = 10^{-3}$ by adding regularization parameter $\gamma = 1.0$ and $\gamma = 10.0$ is not accurate enough. Therefore, the regularization parameter γ is crucial to the accuracy of the energy evolution. In particular, with $\delta t = 10^{-3}$, we observe the energy curve is getting closer to the exact one, when increasing the regularization parameter γ from 0 to 20, i.e. adding a proper regularization parameter would allow the scheme to predict accurate solution with relative bigger time step.

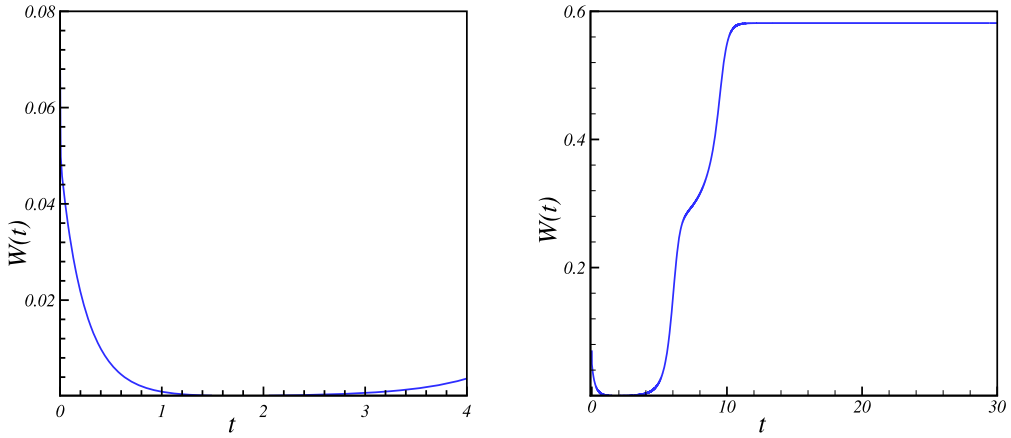

Fig. 4.5. Time evolution of the roughness for the MBE growth model using Crank–Nicolson scheme (3.2). The time step is set at $\delta t = 10^{-3}$ and $\gamma = 20$.

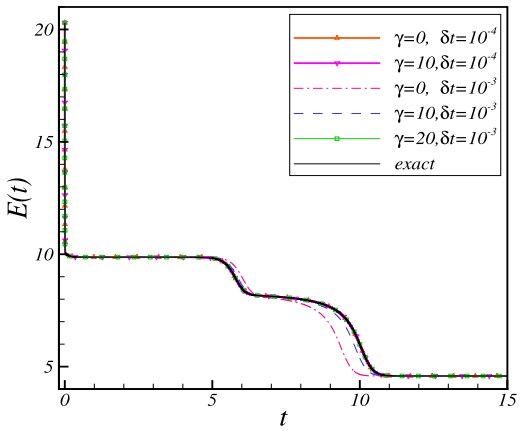

Fig. 4.6. Time evolution of the energy for the MBE growth model using Crank–Nicolson scheme (3.2) when $t \in [0, 15]$ with different time step δt and regularization parameter γ.

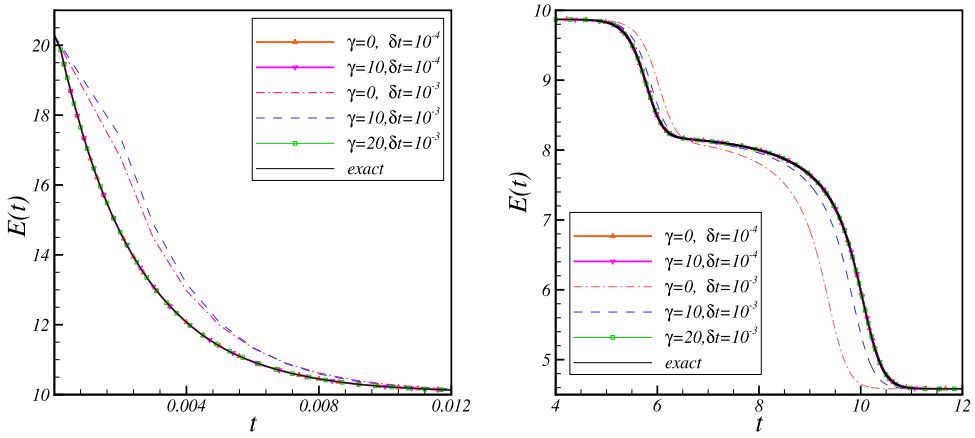

Fig. 4.7. Zoomed plots of time evolution of the energy for the MBE growth model using Crank–Nicolson scheme (3.2) with different time step δt and regularization parameter γ at time region [0, 0.012] (left) and [4, 12] (right) respectively.

Table 4.1
δ_c with different γ for the MBE growth model using Crank–Nicolson scheme (3.2).

γ	0.0	1.0	2.0
δt_c	$0.0006 < \delta t_c < 0.0007$	$0.005 < \delta t_c < 0.006$	$0.01 < \delta t_c < 0.02$
γ	3.0	4.0	5.0
δt_c	$0.05 < \delta t_c < 0.06$	$0.9 < \delta t_c < 1.0$	$\delta t_c > 1$

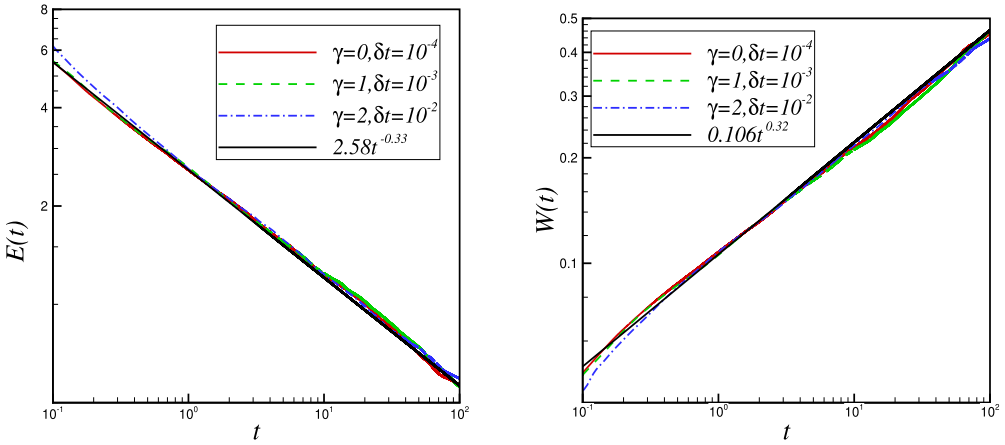

Fig. 4.8. Time evolution of the energy (left) and roughness (right) for the MBE growth model using Crank–Nicolson scheme (3.2) with random number condition when $t \in [0.1, 100]$ respectively.

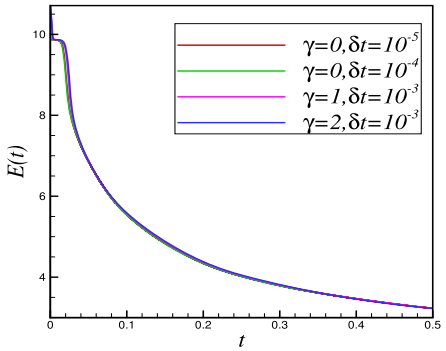

Fig. 4.9. Time evolution of the energy for the MBE growth model using Crank–Nicolson scheme (3.2) with random number condition when $t \in [0, 0.5]$.

4.3. Coarsening dynamics

In this example, we perform numerical simulations of coarsening dynamics in the domain $[0, 12.8] \times [0, 12.8]$. The initial condition is a random state by assigning a random number which varying from -0.001 to 0.001 to each grid points.

The numerical schemes we have proposed are unconditionally stable, which means any time step δt is allowable for the computations of the stability concern. But the global error accumulated in time evolution will lead to the wrong solution, especially with the non-smooth initial condition. However, we will show in this section that the unstable property can be improved by adding the regularization parameter γ. Define δ_c as the largest possible time step which allows stable numerical computation. That is to say, if the time step is greater than δ_c, then the numerical solution will blow up. In Table 4.1, we list the values of δ_c for the MBE growth model using Crank–Nicolson scheme (3.68) with different regularization parameter γ. The semi-discrete scheme (3.2) is approximated by the Fourier spectral methods in space with Fourier mode number $N = 512$. Table 4.1 demonstrate that the improvement on stability and accuracy with the use of γ is significant and the scheme is more accurate when γ is sufficiently large.

In Fig. 4.8, time evolution of the energy (left) and roughness (right) with random number condition when $t \in [0.1, 100]$ are plotted respectively. We observe that the energy decrease approximately like $t^{-\frac{1}{3}}$ and the growth rate of the roughness function is $t^{\frac{1}{3}}$, which is consistent with the result in [28,30]. Also the accuracy of the scheme by adding γ can be checked by Fig. 4.9 which enlarge the energy evolution when $t \in [0, 0.5]$.

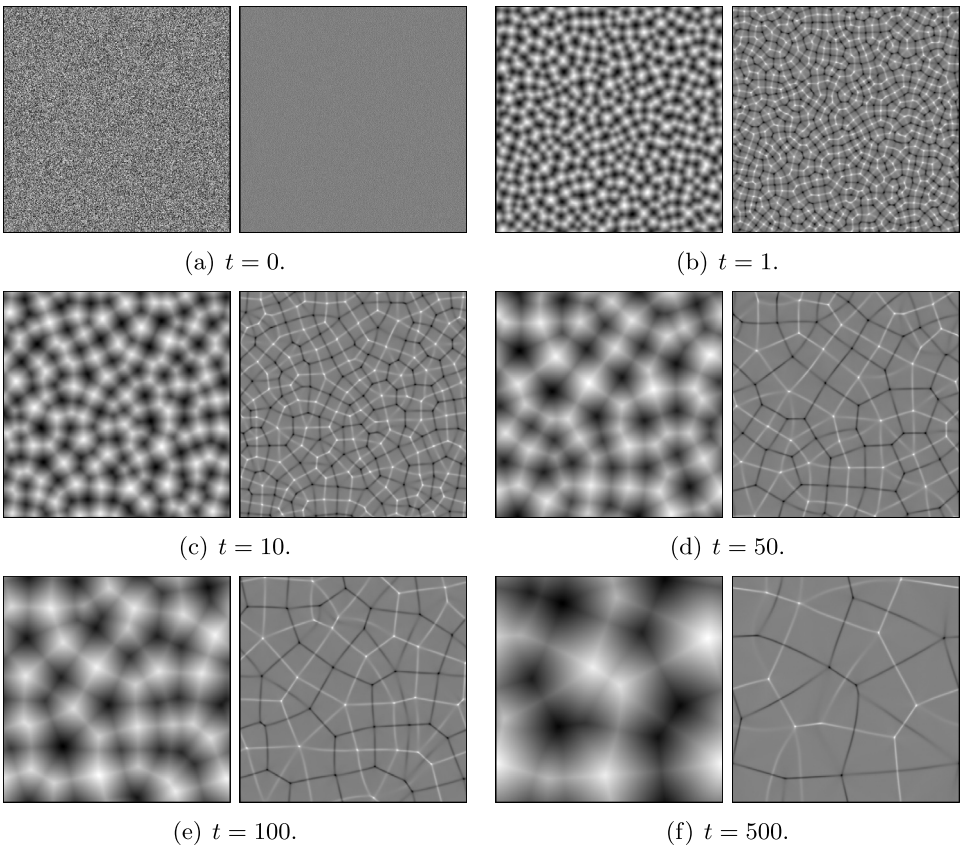

Fig. 4.10. The isolines of numerical solutions of the height function ϕ and its Laplacian $\Delta\phi$ for the MBE growth model with random initial condition. The time step is $\delta t = 0.0001$. Snapshots are taken at $t = 0, 1, 10, 50, 100, 500$, respectively.

The contour lines of numerical solutions of the height function ϕ and its Laplacian $\Delta\phi$ for the MBE growth model with random initial condition are shown in Fig. 4.10. The time step is $\delta t = 0.0001$. Snapshots are taken at $t = 0, 1, 10, 50, 100, 500$, respectively.

5. Conclusion

In this paper, we have proposed two second-order-in-time, spectral-order-in-space full discrete numerical schemes to solve the MBE model. The new schemes are linear, unconditionally energy stable and unique solvable. Thus, it is robust for long time simulations with larger time step and coarser spatial resolution. Several numerical tests are taken to verify our theoretical results. Besides, one novelty in our new scheme is our introducing the regularization parameter. Via numerical comparison, we have shown that, by introducing the regularization parameter, larger time step can also guarantee stability and accuracy. This newly proposed regularized IEQ strategy is also applicable to propose energy stable numerical schemes for a broad class of gradient flow models and/or energy-based thermodynamic consistent models.

Acknowledgement

Lizhen Chen would like to acknowledge the support from National Science Foundation of China through Grant 11671166 and U1530401, Postdoctoral Science Foundation of China through Grant 2015M580038. Jia Zhao would like to acknowledge the support of Research Catalyst Grant from Office of Research and Graduate Studies at Utah State University. Xiaofeng Yang would like to acknowledge the support from National Science Foundation through grant DMS-1720212 and DMS-1418898.

References

[1] S. Badia, F. Guillen-Gonzalez, J. Gutierrez-Santacreu, Finite element approximation of nematic liquid crystal flows using a saddle-point structure, J. Comput. Phys. 230 (2011) 1686–1706.
[2] Y. Bai, Y. Wu, X. Xie, Superconvergence and recovery type a posteriori error estimation for hybrid stress finite element method, Sci. China Math. 59 (2016) 1835–1850.

[3] R.E. Caflisch, M.F. Gyure, B. Merriman, S. Osher, C. Ratsch, D.D. Vvedensky, J.J. Zinck, Island dynamics and the level set method for epitaxial growth, Appl. Math. Lett. 12 (1999) 13–22.
[4] W. Chen, S. Conde, C. Wang, X. Wang, S. Wise, A linear energy stable scheme for a thin film model without slope selection, J. Sci. Comput. 52 (2012) 546–562.
[5] S. Clarke, D.D. Vvedensky, Origin of reflection high-energy electron-diffraction intensity oscillations during molecular-beam epitaxy: a computational modeling approach, Phys. Rev. Lett. 58 (1987) 2235–2238.
[6] R. Duan, Z. Xiang, A note on global existence for the chemotaxis–Stokes model with nonlinear diffusion, Int. Math. Res. Not. 7 (2014) 1833–1852.
[7] David J. Eyre, Unconditionally gradient stable time marching the Cahn–Hilliard equation, in: Computational and Mathematical Models of Microstructural Evolution, San Francisco, CA, 1998, in: Mater. Res. Soc. Symp. Proc., vol. 529, 1998, pp. 39–46.
[8] W. Feng, C. Wang, S. Wise, Linearly preconditioned nonlinear conjugate gradient solvers for the epitaxial thin film equation with slope selection, 2017, pp. 1–15.
[9] W. Feng, C. Wang, S. Wise, Z. Zhang, A second-order energy stable backward differentiation formula method for the epitaxial thin film equation with slope selection, arXiv:1706.01943, 2017.
[10] Y. Gao, X. He, L. Mei, X. Yang, Decoupled, linear, and energy stable finite element method for Cahn–Hilliard–Navier–Stokes–Darcy phase field model, SIAM J. Sci. Comput. 40 (2018) B110–B137.
[11] H. Geng, T. Yin, L. Xu, Perturbation and error analyses of the partitioned LU factorization for block tridiagonal linear systems, J. Comput. Appl. Math. 313 (2017) 1–17.
[12] L. Golubovic, Interfacial coarsening in epitaxial growth models without slope selection, Phys. Rev. Lett. 78 (1997) 90–93.
[13] L. Golubovic, A. Levandovsky, Dislocation dynamics and surface coarsening of rippled states in the epitaxial growth and erosion on (110) crystal surfaces, Phys. Rev. E 77 (2008) 051606.
[14] F. Guillen-Gonzalez, G. Tierra, On linear schemes for a Cahn–Hilliard diffuse interface model, J. Comput. Phys. 234 (2013) 140–171.
[15] F. Guillen-Gonzalez, G. Tierra, Second order schemes and time-step adaptivity for Allen–Cahn and Cahn–Hilliard models, Comput. Math. Appl. 68 (8) (2014) 821–846.
[16] M.F. Gyure, C. Ratsch, B. Merriman, R.E. Caflisch, S. Osher, J.J. Zinck, D.D. Vvedensky, Level-set methods for the simulation of epitaxial phenomena, Phys. Rev. E 58 (3) (1998) 6927–6930.
[17] D. Han, X. Wang, A second order in time uniquely solvable unconditionally stable numerical schemes for Cahn–Hilliard–Navier–Stokes equation, J. Comput. Phys. 290 (1) (2015) 139–156.
[18] S. Jiang, Y. Ou, Incompressible limit of the non-isentropic Navier–Stokes equations with well-prepared initial data in three-dimensional bounded domains, J. Math. Pures Appl. 96 (2011) 1–28.
[19] L. Ju, X. Li, Z. Qiao, H. Zhang, Energy stability and error estimates of exponential time differencing schemes for the epitaxial growth model without slope selection, Math. Comput. (2017), https://doi.org/10.1090/mcom/3262.
[20] H.C. Kang, W.H. Weinberg, Dynamic Monte Carlo with a proper energy barrier: surface diffusion and two-dimensional domain ordering, J. Chem. Phys. 90 (1989) 2824–2830.
[21] J. Krug, Origins of scale invariance in growth processes, Adv. Phys. 46 (1997) 139–282.
[22] H. Lee, J. Shin, J. Lee, A second-order operator splitting Fourier spectral method for models of epitaxial thin film growth, J. Sci. Comput. 71 (3) (2017) 1303.
[23] A. Levandovsky, L. Golubovic, Epitaxial growth and erosion on (001) crystal surfaces: far-from-equilibrium transitions intermediary states, and vertical asymmetry, Phys. Rev. B 69 (2004) 241402.
[24] A. Levandovsky, L. Golubovic, Vertical asymmetry and the ripple-rotation transition in epitaxial growth and erosion on (110) crystal surfaces, Phys. Rev. E 76 (2007) 041605.
[25] A. Levandovsky, L. Golubović, D. Moldovan, Epitaxial growth and erosion on (110) crystal surfaces: structure and dynamics of interfacial states, Phys. Rev. Lett. 89 (26) (2002) 266104.
[26] A. Levandovsky, L. Golubovic, D. Moldovan, Interfacial states and far-from-equilibrium transitions in the epitaxial growth and erosion on (110) crystal surfaces, Phys. Rev. E 74 (1) (2006) 061601.
[27] A. Levandovsky, L. Golubovic, D. Moldovan, Interface dynamics and far-from-equilibrium phase transitions in multilayer epitaxial growth and erosion on crystal surfaces: continuum theory insights, East Asian J. Appl. Math. 1 (2011) 297–371.
[28] B. Li, J.G. Liu, Thin film epitaxy with or without slope selection, Eur. J. Appl. Math. 14 (2003) 713–743.
[29] X. Li, Z. Qiao, H. Zhang, Convergence of a fast explicit operator splitting method for the epitaxial growth model with slope selection, SIAM J. Numer. Anal. 55 (1) (2017) 265–285.
[30] D. Moldovan, L. Golubovic, Interfacial coarsening dynamics in epitaxial growth with slope selection, Phys. Rev. E 61 (2000) 6190–6214.
[31] Z. Qiao, Z. Sun, Z. Zhang, Stability and convergence of second-order schemes for the nonlinear epitaxial growth model without slope selection, Math. Comput. 84 (2015) 653–674.
[32] Z. Qiao, C. Wang, S. Wise, Z. Zhang, Error analysis of a finite difference scheme for the epitaxial thin film model with slope selection with an improved convergence constant, Int. J. Numer. Anal. Model. 14 (2) (2017) 1–23.
[33] Z. Qiao, Z. Zhang, Tao Tang, An adaptive time-stepping strategy for the molecular beam epitaxy models, SIAM J. Sci. Comput. 33 (3) (2011) 1395–1414.
[34] X. Ren, J. Wu, Z. Xiang, Z. Zhang, Global existence and decay of smooth solution for the 2-D MHD equations, J. Funct. Anal. 267 (2014) 503–541.
[35] X. Ren, Z. Xiang, Z. Zhang, Global existence and decay of smooth solutions for the 3-D MHD-type equations without magnetic diffusion, Sci. China Math. 59 (2016) 1949–1974.
[36] M. Schneider, I.K. Schuller, A. Rahman, Epitaxial growth of silicon: a moleculardynamics simulation, Phys. Rev. B 46 (1987) 1340–1343.
[37] J. Shen, C. Wang, X. Wang, S. Wise, Second-order convex splitting schemes for gradient flows with Ehrlich–Schwoebel type energy: application to thin film epitaxy, SIAM J. Numer. Anal. 50 (1) (2012) 105–125.
[38] J. Shen, J. Xu, J. Yang, A new class of efficient and robust energy stable schemes for gradient flows, arXiv:1710.01331, 2017.
[39] J. Shen, J. Xu, J. Yang, The scalar auxiliary variable (SAV) approach for gradient flows, J. Comput. Phys. 353 (2018) 407–416.
[40] J. Shen, X. Yang, An efficient moving mesh spectral method for the phase-field model of two-phase flows, J. Comput. Phys. 228 (2009) 2978–2992.
[41] J. Shen, X. Yang, Numerical approximation of Allen–Cahn and Cahn–Hilliard equations, Discrete Contin. Dyn. Syst. 28 (4) (2010) 1669–1691.
[42] J. Shen, X. Yang, Decoupled energy stable schemes for phase filed models of two phase complex fluids, SIAM J. Sci. Comput. 36 (2014) B122–B145.
[43] J. Shen, X. Yang, Decoupled, energy stable schemes for phase-field models of two-phase incompressible flows, SIAM J. Numer. Anal. 53 (1) (2015) 279–296.
[44] J. Shen, X. Yang, H. Yu, Efficient energy stable numerical schemes for a phase field moving contact line model, J. Comput. Phys. 284 (2015) 617–630.
[45] J. Villain, Continuum models of critical growth from atomic beams with and without desorption, J. Phys. I 19 (42) (1991) 13–22.
[46] C. Wang, X. Wang, S. Wise, Unconditionally stable schemes for equations of thin film epitaxy, Discrete Contin. Dyn. Syst. 28 (1) (2010) 405–423.
[47] C. Wang, S. Wise, An energy stable and convergent finite-difference scheme for the modified phase field crystal equation, SIAM J. Numer. Anal. 49 (3) (2011) 945–969.
[48] Y. Wang, Z. Xiang, Global existence and boundedness in a Keller–Segel–Stokes system involving a tensor-valued sensitivity with saturation: the 3d case, J. Differ. Equ. 261 (2016) 4944–4973.

[49] S. Wise, Unconditionally stable finite difference nonlinear multigrid simulation of the Cahn–Hilliard–Hele-Shaw system of equations, J. Sci. Comput. 44 (2010) 38–68.
[50] S. Wise, C. Wang, J.S. Lowengrub, An energy-stable and convergent finite-difference scheme for the phase field crystal equation, SIAM J. Numer. Anal. 47 (3) (2009) 2269–2288.
[51] C.-Y. Wu, T.-Zh. Huang, Perturbation and error analyses of the partitioned LU factorization for block tridiagonal linear systems, Ukr. Math. J. 68 (2017) 1949–1964.
[52] Y.H. Xia, A fully discrete stable discontinuous Galerkin method for the thin film epitaxy problem without slope selection, J. Comput. Phys. 280 (2015) 248–260.
[53] X. Yang, Error analysis of stabilized semi-implicit method of Allen–Cahn equation, Discrete Contin. Dyn. Syst., Ser. B 11 (2009) 1057–1070.
[54] X. Yang, Linear first and second-order, unconditionally energy stable numerical schemes for the phase field model of homopolymer blends, J. Comput. Phys. 327 (2016) 294–316.
[55] X. Yang, Numerical approximations for the Cahn–Hilliard phase field model of the binary fluid-surfactant system, J. Sci. Comput. (2017), https://doi.org/10.1007/s10915-017-0508-6, in press.
[56] X. Yang, D. Han, Linearly first- and second-order, unconditionally energy stable schemes for the phase field crystal equation, J. Comput. Phys. 333 (2017) 1116–1134.
[57] X. Yang, L. Ju, Efficient linear schemes with unconditional energy stability for the phase field elastic bending energy model, Comput. Methods Appl. Mech. Eng. 315 (2017) 691–712.
[58] X. Yang, L. Ju, Linear and unconditionally energy stable schemes for the binary fluid-surfactant phase field model, Comput. Methods Appl. Mech. Eng. 318 (2017) 1005–1029.
[59] X. Yang, J. Zhao, Q. Wang, Numerical approximations for the molecular beam epitaxial growth model based on the invariant energy quadratization method, J. Comput. Phys. 333 (2017) 102–127.
[60] X. Yang, J. Zhao, Q. Wang, J. Shen, Numerical approximations for a three components Cahn–Hilliard phase-field model based on the invariant energy quadratization method, Math. Models Methods Appl. Sci. 27 (2017) 1993–2023.
[61] R. Zhang, D. Zeng, S. Zhong, Y. Yu, Event-triggered sampling control for stability and stabilization of memristive neural networks with communication delays, Appl. Math. Comput. 310 (2017) 57–74.
[62] J. Zhao, H. Li, Q. Wang, X. Yang, A linearly decoupled energy stable scheme for phase-field models of three-phase incompressible flows, J. Sci. Comput. 70 (2017) 1367–1389.
[63] J. Zhao, Q. Wang, X. Yang, Numerical approximations to a new phase field model for immiscible mixtures of nematic liquid crystals and viscous fluids, Comput. Methods Appl. Mech. Eng. 310 (2016) 77–97.
[64] J. Zhao, Q. Wang, X. Yang, Numerical approximations for a phase field dendritic crystal growth model based on the invariant energy quadratization approach, Int. J. Numer. Methods Eng. 110 (2017) 279–300.
[65] J. Zhao, X. Yang, Y. Gong, Q. Wang, A novel linear second order unconditionally energy-stable scheme for a hydrodynamic Q tensor model for liquid crystals, Comput. Methods Appl. Mech. Eng. 318 (2017) 803–825.
[66] J. Zhao, X. Yang, J. Li, Q. Wang, Energy stable numerical schemes for a hydrodynamic model of nematic liquid crystals, SIAM J. Sci. Comput. 38 (2016) A3264–A3290.
[67] J. Zhao, X. Yang, J. Shen, Q. Wang, A decoupled energy stable scheme for a hydrodynamic phase-field model of mixtures of nematic liquid crystals and viscous fluids, J. Comput. Phys. 305 (2016) 539–556.